A Universal Reduction in Dielectric Response of Confined Fluids

Mohammad H. Motevaselian, and Narayana R. Aluru [1)]

Department of Mechanical Science and Engineering, Beckman Institute for Advanced Science and Technology, University of Illinois at Urbana-Champaign, Urbana, Illinois, 61801, USA

[1)] Corresponding Author/E-mail: aluru@illinois.edu

Abstract

Dielectric permittivity is central to many biological and physiochemical systems as it affects the long-range electrostatic interactions. Similar to many fluid properties, confinement greatly alters the dielectric response of polar liquids. Many studies have focused on the reduction of dielectric response of water under confinement. Here, using molecular dynamics simulations, statistical-mechanical theories and multiscale methods, we study the out-of-plane (z-axis) dielectric response of protic and aprotic fluids confined inside slit-like graphene channels. We show that the reduction in perpendicular permittivity is universal for all the fluids and exhibits a Langevin-like behavior as a function of channel width. We show that this reduction is due to the favorable in-plane (x-y plane) dipole-dipole electrostatic interactions of the interfacial fluid layer. Furthermore, we observe an anomalously low dielectric response under an extreme confinement.

Keywords: confined fluids, dielectric constant, universal reduction, Langevin function, multiscale, molecular dynamics

One of the important fundamental properties of any polar fluid is its dielectric constant. In simple terms, it is the measure of the fluid's ability to screen charges. The knowledge of dielectric permittivity and its influence on electrostatic interactions are of great importance in science and technology. In energy storage devices such as electric double-layer (EDL) capacitors, the amount of energy stored in the device is directly proportional to the solvent dielectric constant, and thus, can be exploited to manipulate the capacitance.[1] In the context of coordination chemistry, dielectric permittivity is an essential component for reactions in the solution *via* changing the solvation free energy barriers.[2] Moreover, solubility and solvation free energy,[3] ion mobility,[4] and molecular transport through nanopores,[5] which are relevant processes in biology[6,7] and water desalination,[8,9] depend strongly on the dielectric permittivity and its variation near interfaces.

Similar to the structural[10,11] and dynamical changes that a fluid undergoes in the vicinity of an interface, the dielectric response of the confined fluid is no longer a scalar quantity (as is the case in the bulk) and is a second ranked tensor exhibiting an anisotropic behavior in different spatial directions (*e.g.,* perpendicular, $\varepsilon_{\perp}$, or parallel, $\varepsilon_{\parallel}$, to a flat interface).[12,13] Such an anisotropic behavior implies a strong preferred directionality for electrostatic interactions[6] and can be very important in understanding dissociation in nanoconfinement,[14,15] dielectrophoretic deposition of carbon nanotubes (CNTs),[16] developing accurate coarse-grained force fields[17] and improving the solvent-implicit approaches often used in biology and continuum theories such as the Poisson-Boltzmann (PB) equation[18] for accurate prediction of capacitance in the electric double-layer capacitors.[19]

Direct measurement of the dielectric permittivity of the fluid under confinement is a very challenging task.[20,21] Previous experiments primarily focused on water and employed different methods and techniques to measure its dielectric response perpendicular to an interface. Thin film

measurements have reported a decrease in the perpendicular dielectric permittivity, $\varepsilon_{\perp}$, of water confined between mica plates as the water slab thickness is reduced from micrometer to nanometer.[22] For the same interface, atomic force microscopy has revealed that water dielectric constant varies from 4 to its bulk value, ε_b =81, within a distance of about 10 nm away from the surface.[23] On the other hand, using the streaming potential method, it was found that the dielectric permittivity of water confined in extended nano spaces is reduced to roughly 1/3 of its bulk value. Recently, capacitance microscopy analyses have revealed that water exhibits an anomalously low out-of-plane dielectric constant of 2.1, when confined between sheets of graphene and hexagonal boron nitride (h-BN). It was also found that the channel width where the water dielectric behavior converges to that of bulk extends up to mesoscales.[21]

Due to the challenges and discrepancies in measuring the dielectric constant from experiments, several computational studies have been performed to study the dielectric permittivity of confined water at various interfaces. As shown in many studies,[20,24] bulk-based relations such as the Kirkwood-Frohlich relation[25,26] should be avoided in calculating the interfacial dielectric permittivity. Using statistical mechanics and linear response theory, fluctuation formulas have been derived to determine the dielectric response of confined polar fluids.[12,13] Using molecular dynamics (MD) simulations, an anomalous dielectric response was found for water confined between ionic Newton black films.[27] Later, it was shown that water exhibits a strong anisotropic dielectric relaxation when confined in graphene nanochannels.[28] This behavior led to an order of magnitude difference in the parallel and perpendicular dipolar fluctuations of water confined between graphene sheets, and was shown to persist even for a 100 nm wide channel.[29] Such anisotropic behavior has also been observed in cylindrical confinement such as in CNTs,[30,31] where the water dielectric constant parallel to the axis of CNT is enhanced while the perpendicular

component is suppressed. This anomalous water dielectric behavior, particularly the reduction in perpendicular dielectric constant of water has also been reported near hydrophobic spheres,[32] soft polar surfaces,[33] and protein surfaces.

Although both computational and experimental studies have been performed on the dielectric permittivity of confined water, there have been only a few studies on non-aqueous solvents. Understanding the dielectric behavior of confined organic solvents is of paramount importance for the application of electrochemical capacitors due to their higher operating voltage thresholds compared to water. In this work, we perform extensive MD and multiscale simulations with cumulative simulation time of 10 μs, to determine the dielectric constant as a function of channel width for water and several technologically relevant organic solvents confined in graphene slit channels. Our study provides fundamental insights into the effect of confinement on perpendicular dielectric permittivity of confined fluids in slit channels of various widths. We observe universal scaling and reduction in the perpendicular dielectric permittivity as a function of the channel width. We demonstrate that the reduction in the out-of-plane dielectric permittivity exhibits a Langevin-like behavior. The reason behind this reduction is attributed to the favorable in-plane dipole-dipole interactions. Moreover, we find that the perpendicular dielectric permittivity is anomalously low in sub-nanometer channels. Finally, we introduce a multiscale parallel-plate capacitor model to calculate the perpendicular permittivity of the confined fluids. The model is more robust than the fluctuation formula (requires only two short MD simulations of about 4 ns) and its prediction of the perpendicular dielectric permittivity, in the limit of zero external electric field, agrees well with the result of the fluctuation formula.

Results and Discussion

Bulk dielectric permittivity and dipolar strength. In general, solvents can be classified into two categories: protic and aprotic. The former refers to the solvents capable of forming H-bonds, whereas the latter refers to solvents which cannot accept or donate a hydrogen bond. The set of fluids considered in this study have dielectric constant (calculated from MD simulations) ranging from ~9 (non-polar aprotic fluid such as dichloromethane) to intermediate values of ~25 (polar protic and aprotic fluids such as methanol and acetonitrile, respectively) and to the highly polar protic fluid such as water (SPC/E) with the dielectric constant of ~71. In addition to their technological relevance and wide range of dielectric permittivity, the selection of these solvents shows an interesting connection between bulk dielectric permittivity, proticity and dipolar strength. Assuming periodic tinfoil (conducting metal) boundary conditions, the bulk dielectric permittivity can be expressed *via* the following relation:[34,35]

$$\varepsilon_{\mathrm{b}} = 1 + 3C_{\mathrm{d}}G_{\mathrm{k}} \tag{1}$$

In eq (1), G_{k} is the Kirkwood factor, representing the angular dipolar correlations among the dipoles (*e.g.,* for uncorrelated dipoles G_{k} is equal to 1), and C_{d} is the dipolar strength given by,

$$C_{\mathrm{d}} = \frac{\rho_{\mathrm{b}}\mu^2}{9\varepsilon_0 k_{\mathrm{B}}T} \tag{2}$$

where μ, ρ_{b}, ε_0, k_{B}, and T are the dipole moment, bulk density, vacuum permittivity, Boltzmann constant and temperature, respectively. We observe that for a similar value of dipolar strength the hydrogen-bonded liquids have a higher dielectric permittivity compared to the non-hydrogen-bonded liquids (see Supplementary Table S1). This suggests larger G_{k} values, hence, stronger dipolar correlations and alignments in protic liquids. Thus, we investigate the effect of confinement on the dielectric response of both protic and aprotic solvents with distinct dipolar strengths.

Perpendicular dielectric permittivity of confined liquids. A typical simulation box consists of fluid molecules sandwiched between two flat graphene sheets separated by a distance, H (see Supplementary, Figure S1). For each channel width, we use the fluctuation formula (see eq (9) in the Methods Section) to compute the spatially varying perpendicular dielectric permittivity and average it over the entire channel width (see the Methods Section), which makes it easier to compare with experiments and suitable for coarse-grained modeling and analytical approaches. The size of the confinement (H) investigated ranges from large channels with a well-formed bulk-like region away from the walls to smaller channels where no bulk-like region can be identified and to extremely narrow channel widths of a few Angstroms, where an accurate determination of the solvent dielectric constant requires high resolution experiments to reduce noise and error bar. Moreover, such small-sized carbon slit-pores of width 0.6-1 nm (less than the size of solvated ions) have exhibited anomalously high capacitance which contradicts the traditional understanding of supercapacitors.[36,37]

For all the channel widths and different fluids considered, we observe a reduction in the perpendicular permittivity compared to the bulk value (Figure 1). The reduction in permittivity with size, however, varies for different fluids. At large channel widths (with a well-defined bulk-like region), the dielectric constant reduces in a nonlinear fashion from the bulk value and continues to decrease in an almost linear fashion for narrower channel widths (with no bulk-like region). For the confinement of width H_{sl} (the smallest channel width considered in our simulations), where only a single layer of fluid could fit inside the channel (see Supplementary, Figure S2), the corresponding dielectric constant, $\varepsilon_{\mathrm{sl}}$ is exceptionally small. For some of the fluids, such as dichloromethane, this value is close to 1. This indicates that at small separation distances, the ability of fluids (both protic and aprotic) to screen charges normal to the surface is substantially

inhibited. We note that due to the lack of electronic degrees of freedom, the high frequency limit dielectric permittivity, ε_∞, is equal to unity for non-polarizable force fields[38] (see the Methods section for different force fields). Thus, the value of $\varepsilon_{\mathrm{sl}}$ for all the fluids lies above $\varepsilon_\infty = 1$. To the best of our knowledge, with the exception of water, there are no relevant experimental studies on the variation of dielectric permittivity of non-aqueous fluids as a function of the channel width. Nevertheless, our results are in good agreement with recent experiments reported on the confined water dielectric permittivity.[21] For water, both simulations and experiments show a linear reduction in perpendicular permittivity for small channels and a nonlinear reduction from the bulk value for larger channel widths. The smallest permittivity found in experiment was ~2.1 ± 0.2 for channel widths smaller than 2 nm. In our simulations, however, we observe such a low value of perpendicular dielectric permittivity only in sub-nanometer channels.

Our results show that the reduction in the perpendicular dielectric permittivity is not exclusive to water, rather it is a universal feature for the confined fluid systems. As a corollary, electrostatic interactions perpendicular to an interface are enhanced under confinement. In other words, the electrostatic repulsion or attraction becomes stronger between two similar or oppositely charged surfaces. This phenomenon can be very important in biology due to the polar nature of protein surfaces and their interaction with water or in energy storage applications as the dielectric permittivity of solvents can drastically impact the capacitance of a device.

Langevin behavior of the perpendicular permittivity. As depicted in Figure 1c, the behavior of the perpendicular permittivity as a function of the channel width can be approximately modeled by a Langevin function as,

$$\varepsilon_\perp(H) = \varepsilon_{\mathrm{sl}} + \Delta\varepsilon\, \mathcal{L}\left(3\frac{H - H_{\mathrm{sl}}}{\sigma_{\mathrm{d}}\Delta\varepsilon}\right) \tag{3}$$

where $\Delta\varepsilon = (\varepsilon_{\mathrm{b}} - \varepsilon_{\mathrm{sl}})$, $\mathcal{L}(x) = \coth(x) - \frac{1}{x}$ is the Langevin function, and σ_{d} is an effective length scale which is determined from the slope at small channel widths.

In the context of dielectric theory, Langevin function has also been used to describe the orientational polarization of the system of non-interacting dipoles, the dielectric saturation effects due to the external electric field,[39–41] dielectric decrement as a function of ion concentration,[42,43] and to model an effective permittivity in classical theories such as the Poisson-Boltzmann theory.[44]

For small channels, especially in the limit of $H \to H_{\mathrm{sl}}$, the behavior of the perpendicular dielectric permittivity is approximately linear as a function of the channel width with the slope directly related to σ_{d} (see Supplementary, Figure S3). The resultant values for σ_{d} are very similar to the effective molecular diameter of the fluids considered[45] (Table 1). In addition, knowing σ_{d} for each fluid and using eq (3), we can predict the characteristic length scale, λ_{b}, for which the bulk dielectric behavior is recovered (Table 1). The criterion used to calculate λ_{b} was that the perpendicular dielectric permittivity at $H = \lambda_{\mathrm{b}}$ reaches 99% of ε_{b}. We found that λ_{b} ranges from hundreds of nanometers for dichloromethane, methanol, and acetonitrile to micrometers for water. Our results for water, agree well with the recent experiments[21] and previous MD simulations, showing that the effect of confinement on the dielectric response of water extends up to mesoscale dimensions.[46] We emphasize that these length scales are obtained for fluids confined in the graphene slit-pores and these length scales can change as the substrate changes.

By rearranging eq (3) and plotting the scaled perpendicular dielectric permittivity, $\tilde{\varepsilon}_{\perp} = \frac{\varepsilon_{\perp} - \varepsilon_{\mathrm{sl}}}{\varepsilon_{\mathrm{b}} - \varepsilon_{\mathrm{sl}}}$, against the scaled channel width, $\widetilde{H} = \frac{H - H_{\mathrm{sl}}}{\sigma_{\mathrm{d}}(\varepsilon_{\mathrm{b}} - \varepsilon_{\mathrm{sl}})}$, it is apparent that all the data for different fluids approximately collapses onto a single curve including the experimental measurements reported in the literature for water out-of-plane dielectric permittivity.[21] This relationship between the scaled

perpendicular dielectric permittivity and the scaled channel width can be modeled by the Langevin function, *i.e.,* $\tilde{\varepsilon}_{\perp}(\widetilde{H}) = \mathcal{L}(3\widetilde{H})$.

Multiscale parallel-plate capacitor model for dielectric permittivity. A simple capacitor consists of a dielectric medium sandwiched between two electrodes of equal and opposite charges ($\pm Q$) separated by a distance H. A capacitor can be characterized by its capacitance (C) which is a measure of the amount of charge stored for a given potential difference across its electrodes, *i.e.,*

$$C = \frac{Q}{\Delta\Phi} = \frac{\sigma_{\mathrm{c}} A}{\Delta\Phi} \tag{4}$$

where σ_{c} is the electrode surface charge density, A is the surface area of the electrode, and $\Delta\Phi = \Phi_{\mathrm{anode}} - \Phi_{\mathrm{cathode}}$ with anode and cathode referring to the positive and negative electrodes, respectively. On the other hand, from a theoretical point of a view, the capacitance for a conventional parallel-plate capacitor can be written in terms of the geometry of the capacitor and the dielectric permittivity of the confined medium as,

$$C = \frac{A\varepsilon_0\varepsilon_{\mathrm{r}}}{H} \tag{5}$$

Using eqs (4) and (5), the dielectric permittivity of the medium can be expressed as,

$$\varepsilon_{\mathrm{r}} = \frac{\sigma_{\mathrm{c}} H}{\varepsilon_0 \Delta\Phi} \tag{6}$$

Herein, in addition to the fluctuation formula to calculate the perpendicular permittivity, we have simulated capacitor channels, where uniform partial charges, positive on the right wall ($z = H$) and negative on the left wall ($z = 0$), were assigned to the wall atoms to achieve an external electric field of strength, $E_{\mathrm{ext}} = \sigma_{\mathrm{c}}/\varepsilon_0$. Thus, by knowing the electrostatic potential of the anode and cathode, the dielectric permittivity of the confined medium, which coincides with the perpendicular dielectric permittivity (*i.e.,* $\varepsilon_{\mathrm{r}} = \varepsilon_{\perp}$), can be obtained using eq (6). To find the

electrostatic potential for a confined fluid system, we first calculated the atomic charge density profile from MD simulations and used the Poisson equation with the proper boundary conditions (see the Methods Section) to obtain the electrostatic potential. The schematic of the entire procedure for water is shown in Figure 2a.

Compared to the fluctuation formula which is only applicable in the absence of an external electric field and requires long and tedious equilibrium simulations, eq (6) is more robust and can be used to calculate the electric-field-dependent perpendicular dielectric permittivity. However, one caveat is that it cannot be used at zero external electric field. To address this limitation and to establish verification of the results of eq (6) with the fluctuation formula, we investigated the variation of the perpendicular dielectric permittivity as a function of the electric field (Figure 2c). In general, as the electric field increases, the fluid dipoles get more aligned with the applied field, and thus, result in a lower dielectric permittivity. At weaker electric fields, however, it is clear that the slope plateaus indicating an almost constant dielectric permittivity. This is not surprising, as on the basis of the linear response theory, for weak enough electric fields the response of the fluid total polarization density ($p_\perp$) varies linearly with the local electric field ($E_\perp$), *i.e.,* $p_\perp = \varepsilon_0(\varepsilon_\perp - 1)E_\perp$. This is evident in the inset of Figure 2b. It can be seen that for water, the linear regime is observed for $E_{\text{ext}} \leq 0.2$ VÅ^{-1}, which is consistent with prior literature for water confined in graphene channels.[19] To extract the zero field perpendicular dielectric permittivity, we used the Booth relation[39,40] for the electric field-dependent perpendicular dielectric permittivity,

$$\varepsilon_\perp(E_{\text{ext}}) = n^2 + \frac{3(\varepsilon_\perp(0) - n^2)}{bE_{\text{ext}}}\mathcal{L}(bE_{\text{ext}}) \tag{7}$$

where n is the refractive index, which is related to the infinite frequency dielectric constant by $\varepsilon_\infty = n^2$. In eq (7), b and $\varepsilon_\perp(0)$ are the fitting parameters for our data and $n = 1$ due to the use of

non-polarizable SPC/E forcefield. Figure 2c shows that eq (7) can extract $\varepsilon_{\perp}$ in the limit of zero electric field. For each channel width, we only perform 2 non-equilibrium MD (NEMD) simulations at two distinct electric fields to obtain the perpendicular dielectric permittivity *via* eq (6), and subsequently use eq (7) to extract the zero electric field perpendicular dielectric permittivity. The results are illustrated in Figure 2d, which show a good agreement with the perpendicular dielectric permittivity obtained from the fluctuation formula. Therefore, the aforementioned multiscale method eliminates the need for long and tedious simulations required to calculate the perpendicular dielectric permittivity from the fluctuation formula. It is worth mentioning that we can further modify eq (7) to account for the dielectric saturation in the limit of very high external electric fields and consequently obtain an accurate representation of the perpendicular dielectric permittivity as a function of the external electric field (see Supplementary, Figure S4).

Dipole correlations and reduced perpendicular permittivity. It is widely accepted that the low perpendicular dielectric permittivity is due to a dielectric dead layer (low permittivity interfacial region) at the fluid-solid interface.[47,48] However, the origin of such a low dielectric layer is still debated as to whether it is intrinsic to the dielectric medium or due to the impurities on the surface.[49] In either case, the existence of a dead layer will lower the overall dielectric constant, thus, having a huge impact on the capacitance of the medium.[4,49] It has been shown for water that the reduction in permittivity is attributed to the favorable in-plane hydrogen-bond network at the solid surface, which makes it difficult for molecules to re-orient in the perpendicular direction and respond to the external field.[50] However, our results indicate that not only protic fluids such as water or methanol (hydrogen bonding fluids) but also aprotic fluids exhibit a low out-of-plane dielectric permittivity under confinement, suggesting that the underlying mechanism for the

reduction in permittivity is not just due to the hydrogen bond network effect in the interfacial layer (IFL). Since the main contribution to the static dielectric permittivity of polar fluids is the orientational polarizability (compared to the electronic polarizability),[51] and the dominant term is the dipole polarization, we investigate the in-plane dipole orientational correlations in the first fluid density layer (interfacial layer) adjacent to the wall (see Supplementary Figure S5). As depicted in Figure 3a-d, for all the fluids considered, compared to the bulk, the in-plane dipole-dipole correlation, $h_{\Delta}(r)$ (see the Methods Section for definition) is enhanced, showing the tendency of the dipoles to lay parallel to the graphene surface. Such a preferred orientation was reported for polar liquids on graphene.[51] This preferred orientation can be understood by analyzing the in-plane dipole-dipole electrostatic energy of the interfacial layer, which can be written as,

$$U_{\mathrm{elec,dd}} = -\frac{AL_{\mathrm{IFL}}^2\rho_{\mathrm{IFL}}^2}{2\varepsilon_0}\mu^2\int_0^{\infty}\frac{h_{\mathrm{D}}(r_{\parallel})}{r_{\parallel}^2}dr_{\parallel} \qquad (8)$$

where h_{D} represents the angular dependence of the dipole-dipole interaction energy (see the Methods Section for mathematical definition), $r_{\parallel}$ is the in-plane separation distance between the dipoles, L_{IFL} is the width of the interfacial layer, and ρ_{IFL} is the density of the molecules in the interfacial layer. Figure 3e-h shows the correlation function $h_{\mathrm{D}}(r)$ for different fluids. Similar to the in-plane dipole-dipole correlation, $h_{\mathrm{D}}(r)$ is enhanced next to the interface and it is dominantly positive, suggesting that the preferred alignment of dipoles is to lower the dipole-dipole interaction energy. In addition to $h_{\mathrm{D}}(r)$, we expect that the density and the dipole moment play an important role as they explicitly enter eq (8). Using all these parameters, we have calculated the in-plane electrostatic energy for water, methanol, dichloromethane and acetonitrile (Table 2). We note that water has the lowest energy followed by acetonitrile and methanol (similar values), and dichloromethane has the highest in-plane dipole-dipole electrostatic energy. This explains the

anomalous reduction in the perpendicular permittivity and the order in which this reduction occurs relative to the bulk permittivity, $\varepsilon_{\perp}(H)/\varepsilon_{\mathrm{b}}$ (Water > Methanol ≈ Acetonitrile > Dichloromethane) (Figure 1b). Overall, our results show that the reduction in perpendicular dielectric permittivity ensues from the existence of confinement and the tendency of the fluid molecules to align parallel to the graphene surface. The preferred in-plane alignment of molecules lowers the dipole-dipole electrostatic interaction energy hindering the out-of-plane rotation and thus reducing the tendency to align with an external electric field acting in the normal direction (z-axis).

Conclusions

Till date, most of the literature on perpendicular dielectric permittivity dealt with confined water and less attention has been given to the response of other polar liquids. Many studies have shown that the perpendicular dielectric response is significantly reduced as a result of confining water molecules. This work goes further by demonstrating that the reduction in the perpendicular permittivity is a universal feature for both protic and aprotic fluids. The physical origin of this reduction was attributed to the low dielectric response of the interfacial layer due to the preferred in-plane alignment of the fluid molecules' dipole moments. Such an alignment lowers the in-plane dipole-dipole electrostatic energy and therefore, restricts the molecular rotations normal to the surface. Furthermore, our results reveal that for narrow confinements with no bulk-like region in the middle of the channel, perpendicular permittivity scales linearly as a function of the channel width and the slope is proportional to an effective length scale which is close to the fluid's molecular diameter. As the bulk-like region begins to form inside the channel, nonlinear effects are observed. We showed that such a behavior can be modeled by the Langevin function. Moreover, using the Langevin function we predict the length scale beyond which the fluid can be treated as bulk in terms of its dielectric properties. We found that depending on the fluid, the

channel width that recovers the bulk dielectric response varies from hundreds of nanometers for less polar molecules such as dichloromethane to micrometers for water. Our results for water are in qualitative agreement with the recent capacitance microscopy experiments in which the length scale to retrieve bulk-like dielectric permittivity was estimated to be beyond 100 nm.

Under extreme confinement (sub nanometer channels), the perpendicular permittivity of the fluids is anomalously suppressed to values as low as < 2.5. This indicates that the molecules primarily take a planar orientation on the surface with very small out-of-plane dipolar components. For water the smallest value of the perpendicular permittivity was found to be ~2.3 in good agreement with the experimental value of ~2.1.[21] Using the multiscale parallel-plate capacitor model, we have also studied the perpendicular response of water dielectric permittivity as a function of the external electric field. In the limit of a vanishingly small electric field, our results coincide with the perpendicular dielectric permittivity obtained from the statistical mechanics approach (fluctuation formula). Furthermore, we observed a non-monotonic decrease in the out-of-plane dielectric permittivity as a function of the electric field. We showed that such a dielectric decrement can be adequately modelled by the Booth relation.[39,40]

We believe our findings will provide significant implications for theoretical assessment of both protic and aprotic solvents next to an interface, understanding long-ranged electrostatic interactions in biological systems, and understanding the solvation chemistry in polar fluids. Finally, it would be interesting to see whether our predictions for the reduction in perpendicular permittivity of both protic and aprotic fluids confined in slit channels could be verified in actual experiments of such systems.

Methods

Molecular dynamics simulations. All the MD simulations were performed using the GROMACS software.[52] Equations of motion are integrated with the leap-frog algorithm with a time step of 1 fs. During the simulations, temperature is kept constant at 298 K using the Nosé-Hoover thermostat[53] with a 0.2 ps time constant. For the bulk simulations, all systems were initially equilibrated for 5 ns, followed by a 20 ns of production run in isothermal-isobaric (NPT) ensemble with the pressure of 1 bar. For the short-ranged interactions, the cutoff radius was set to 1.2 nm. Both energy and pressure tail corrections[54] have been applied to the standard 12-6 LJ potential for the bulk MD simulations. For the bulk MD simulations, the long-range electrostatic interactions were calculated using the particle mesh Ewald (PME) summation[55] with the tinfoil boundary condition (infinite dielectric) and a fast Fourier transform (FFT) grid spacing of 0.12 nm. Periodic boundary conditions were applied in all the directions. In order to obtain enough statistics to calculate the bulk dielectric permittivity, trajectories of atoms were collected every 0.05 ps. For the confined fluid simulations, all simulations were performed in the canonical ensemble (NVT). Confined systems consist of two parallel graphene sheets separated by a distance of H in the z direction and the lateral dimensions lie in the x-y plane with an area of 4.17648×4.25420 nm^2. The LJ length and energy scale parameters for the carbon atoms are 0.3390 nm and 0.2334 kJ/mol, respectively. During the simulation, the graphene sheets were frozen, *i.e.,* their positions were not updated. The system is periodic in all directions with an extra empty space (vacuum) of length at least $3H$ added in the z direction (see Supplementary, Figure S6). Although periodic in the z direction, we exclude the long-ranged electrostatic contributions from the periodic image cells, which are unwanted in the two dimensional periodic systems (2DP). Yeh and Berkowitz[56] have shown that such a treatment of the electrostatic interactions (*i.e.,* Ewald3dc) mimics the behavior

of rigorous two-dimensional Ewald summation for a 2DP system with a finite length along the third dimension. Therefore, by eliminating the contributions from the image cells in the z direction and sufficient empty space in the z direction, the right fluctuation formula to calculate the perpendicular dielectric permittivity under these conditions is eq (9).

In this study, we have considered a total of 4 fluids of various polarity and density such as water, methanol, acetonitrile, and dichloromethane. We modeled water by the extended simple point charge model (SPC/E) and used the SHAKE algorithm[57] to maintain the molecule rigidity. For acetonitrile, we adopted the six-site model from Nikitin *et al*.,[58] where the force field parameters were optimized to reproduce the dielectric permittivity close to the experimental value. For the rest of the fluids, all parameters were adopted from the All-Atom Optimized Potential for Liquid Simulations (OPLS-AA) forcefield[59] with the exception of dichloromethane charges, which were modified for more accurate estimation of its dielectric constant.[60] Quantum, atomic and electronic polarizability effects are neglected, therefore, the fluid models are considered to be non-polarizable. In order to determine the number of confined fluid particles, each channel was connected to a big reservoir equilibrated at the temperature of 298 K and the pressure of 1 bar, to allow for particle exchange in an NVT ensemble. To obtain enough statistics, especially for calculating the perpendicular dielectric permittivity, the equilibrium properties are averaged over a set of 7 MD simulations each with different initial velocities and positions for a total time of 20 ns, in which the first 5 ns were discarded. Additionally, we have simulated water in capacitor channels, where uniform partial charges are assigned to the atoms of each wall to achieve external electric fields of 0.005, 0.01, 0.02, 0.05, 0.1, 0.2, 0.3, 0.5, 0.7, 1.0, and 1.5 $\mathrm{V\AA^{-1}}$.

Fluctuation formula for perpendicular permittivity. Unlike bulk, in confinement, the dielectric permittivity of a polar fluid takes a tensorial form. For a slit-channel, where the

inhomogeneity is only in one direction (perpendicular to the surface, z axis), the component of the dielectric permittivity tensor spatially varies as a function of z. Using statistical mechanics and the linear response theory,[12,13] the locally varying inverse perpendicular permittivity is given *via* the following fluctuation formula,

$$\varepsilon_{\perp}^{-1}(z) = 1 - \beta\varepsilon_0^{-1}[\langle p_{\perp}(z)P_{\perp}\rangle_0 - \langle p_{\perp}(z)\rangle_0\langle P_{\perp}\rangle_0] \tag{9}$$

where β is the inverse of thermal energy, $\langle\cdots\rangle_0$ denotes the ensemble average in the absence of an external electric field, $p_{\perp}(z)$ is the perpendicular fluid polarization density at position z, and $P_{\perp}$ is the perpendicular component of the fluid total polarization and is given by,

$$P_{\perp} = A\int_0^H p_{\perp}(z)dz \tag{10}$$

It has been shown that in addition to the dipole moment, higher-order multipole moments such as quadrupole and octupole moments have a non-negligible contribution to the perpendicular dielectric permittivity.[13] Therefore, to account for higher-order multipole moments the perpendicular polarization density at position z is calculated as,

$$p_{\perp}(z) = \int_0^z \rho_{\mathrm{e}}(z')dz' \tag{11}$$

where $\rho_{\mathrm{e}}(z)$ is the fluid atomic charge density profile in the z direction, and is computed by the binning method with 0.1 Å resolution. Integrating eq (9) over the entire channel yields the average inverse perpendicular permittivity as,

$$\varepsilon_{\perp}^{-1} = 1 - \frac{\langle P_{\perp}^2\rangle - \langle P_{\perp}\rangle^2}{\varepsilon_0 V k_{\mathrm{B}}T} \tag{12}$$

We want to emphasize that eq (9) was originally derived for a single slab, periodic only in the x and y directions.[12] For a system non-uniform in the z direction, but periodic in all directions (*e.g.,* a solvated lipid bilayer), the correct fluctuation formula to calculate the perpendicular dielectric

permittivity should also include the fluctuations of the total polarization of the system.[61] For more information, see Supplementary information Section S5.

Electrostatic potential calculations. To compute the electrostatic potential, $\Phi(z)$, of the confined fluid in a slit channel, the Poisson equation is used which is given by

$$\frac{d^2\Phi}{dz^2} = -\frac{\rho_e(z)}{\varepsilon_0} \tag{13}$$

with the following boundary conditions:

$$\left.\frac{d\Phi}{dz}\right|_{z=0} = -\frac{\sigma_{\mathrm{c,left}}}{\varepsilon_0} \tag{14-a}$$

$$\left.\frac{d\Phi}{dz}\right|_{z=H} = +\frac{\sigma_{\mathrm{c,right}}}{\varepsilon_0} \tag{15-b}$$

$$\Phi(z = H/2) = 0 \tag{16-c}$$

where $\sigma_{\mathrm{c,left}} = -\sigma_c$ and $\sigma_{\mathrm{c,right}} = +\sigma_c$ are the surface charge densities on the left and right wall, respectively. We note that, due to the last boundary condition (eq (16-c)), the electrostatic potential at any point is relative with respect to the mid-point of the channel.

Dipolar orientational correlation functions. For a system of dipolar molecules the two important orientational correlations are the dipole-dipole pair correlation, $h_{\Delta}(r)$, and $h_{\mathrm{D}}(r)$ which represents the angular dependence of the dipole-dipole interaction energy. In MD simulations, $h_{\Delta}(r)$ and $h_{\mathrm{D}}(r)$ can be calculated using the following equations:

$$h_{\Delta}(r) = \frac{1}{\mathrm{N}\rho_{\mathrm{b}}}\left\langle \sum_{\mathrm{i}=1}^{\mathrm{N}} \sum_{\mathrm{j}\neq 1}^{\mathrm{N}} \widehat{\boldsymbol{\mu}}_{\mathrm{i}} \cdot \widehat{\boldsymbol{\mu}}_{\mathrm{j}}\, \delta\left(\boldsymbol{r} - \boldsymbol{r}_{\mathrm{ij}}\right)\right\rangle \tag{17}$$

$$h_{\mathrm{D}}(r) = \frac{1}{\mathrm{N}\rho_{\mathrm{b}}}\left\langle \sum_{\mathrm{i}=1}^{\mathrm{N}} \sum_{\mathrm{j}>\mathrm{i}}^{\mathrm{N}} \left[3\left(\widehat{\boldsymbol{\mu}}_{\mathrm{i}} \cdot \hat{\boldsymbol{r}}_{\mathrm{ij}}\right)\left(\widehat{\boldsymbol{\mu}}_{\mathrm{j}} \cdot \hat{\boldsymbol{r}}_{\mathrm{ij}}\right) - \widehat{\boldsymbol{\mu}}_{\mathrm{i}} \cdot \widehat{\boldsymbol{\mu}}_{\mathrm{j}}\right] \delta\left(\boldsymbol{r} - \boldsymbol{r}_{\mathrm{ij}}\right)\right\rangle \tag{18}$$

where N is the number of dipolar molecules, $\boldsymbol{r}$ is the position vector with magnitude of r, $\boldsymbol{r}_{ij} = \boldsymbol{r}_j - \boldsymbol{r}_i$ is the center-to-center distance between i and j dipoles with the magnitude of r_{ij}, and $\widehat{\boldsymbol{\mu}}$ is the unit vector in the direction of $\boldsymbol{\mu}$, which represents the molecular dipole moment vector**.**

Acknowledgement

The work on the estimation of the perpendicular dielectric permittivity of water was supported by the Center for Enhanced Nanofluidic Transport (CENT), an Energy Frontier Research Center funded by the U.S. Department of Energy, Office of Science, Basic Energy Sciences (Award # DE-SC0019112). The other aspects of the work presented here were supported by the National Science Foundation under Grants 1545907, 1708852, 1720633, and 1921578. The computing power was provided by the Extreme Science and Engineering Discovery Environment (XSEDE) granted by National Science Foundation (NSF) Grant No. OCI1053575 and Blue Waters supercomputing center, awarded by the state of Illinois and NSF, OCI-0725070, ACI-1238993.

Supporting Information

Schematic illustration of the simulation setup (Section S1), center-of-mass number density of confined fluids (Section S2), linear variation of the perpendicular dielectric permittivity as a function of the channel width for narrow width slit channels (Section S3), variation of perpendicular dielectric permittivity with external electric field (Section S4), interfacial density layers for different fluids (Section S5), effect of the electrostatic treatment and boundary conditions in MD simulations on the calculation of perpendicular dielectric permittivity (Section S6) and data regarding the bulk permittivity, Kirkwood factor, and dipolar strength (Section S7).This material is available free of charge *via* the Internet at http://pubs.acs.org.

Table 1. Anomalously low perpendicular dielectric permittivity of different fluids in sub-nanometer slit channels. σ_d is the fitting parameter in the Langevin equation, λ_b is the length scale to retrieve the bulk dielectric behavior, and σ_a is the effective molecular diameter taken from Ref.[45]

Fluid	$H_{\mathrm{sl}}(\mathrm{nm})$	$\varepsilon_{\mathrm{sl}}$	$\sigma_{\mathrm{d}}(\mathrm{nm})$	$\sigma_a(\mathrm{nm})$	$\lambda_{\mathrm{b}}(\mathrm{nm})$
Water	0.634	2.3146	0.3370	0.2922	1035.8
Methanol	0.700	1.5800	0.3870	0.3835	288.0
Acetonitrile	0.800	2.0900	0.5501	0.4244	344.5
Dichloromethane	0.700	1.0558	0.6318	0.5045	153.0

Table 2. The dipole moment squared, bulk and the interfacial layer densities, and the in-plane dipole-dipole electrostatic potential for various fluids.

Fluid	$\mu^2(\mathrm{D}^2)$	$\rho_{\mathrm{b}}\ (\mathrm{nm}^{-3})$	$\rho_{\mathrm{IFL}}(\mathrm{nm}^{-3})$	$U_{\mathrm{dd,elec}}(\mathrm{kJ\ mol}^{-1})$
Water	5.5225	33.40	62.24	-1475.92
Methanol	5.4820	14.58	39.04	-281.09
Acetonitrile	15.1632	11.47	26.88	-316.04
Dichloromethane	4.9131	8.96	24.59	-52.53

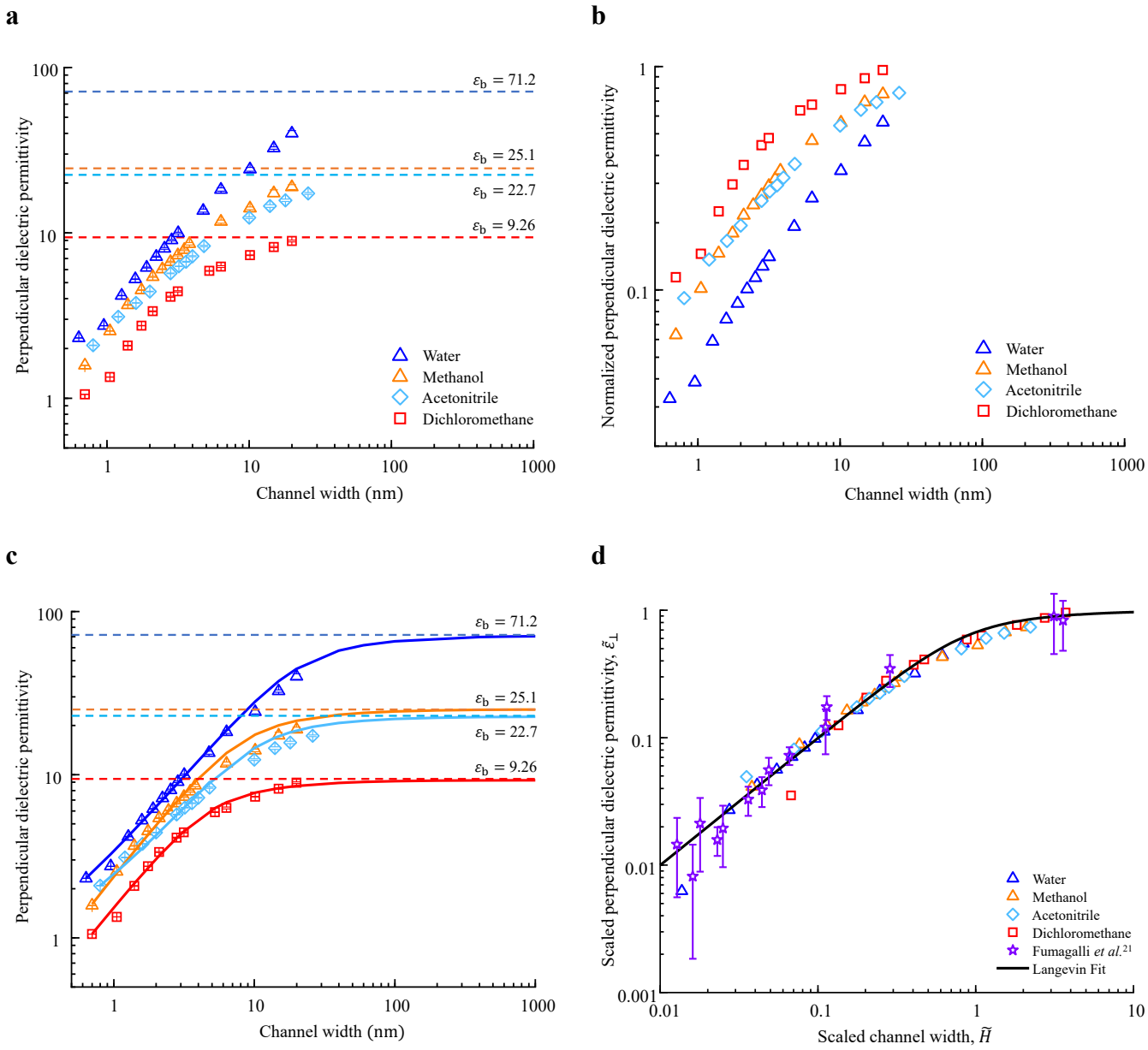

Figure 1. **Perpendicular dielectric permittivity of confined fluids**. **(a)** Perpendicular dielectric permittivity of different fluids confined in graphene slit-like channels of various widths. The bulk dielectric constant for each fluid is shown by the dashed horizontal lines and the value is denoted by ε_b. **(b)** Perpendicular dielectric permittivity normalized by the bulk dielectric constant of each fluid as a function of the channel width, *i.e.,* $\varepsilon_\perp(H)/\,\varepsilon_b$. **(c)** Langevin-like behavior of the perpendicular dielectric

permittivity as a function of the channel width according to eq (3). **(d)** Using proper scaling, the data for the perpendicular dielectric permittivity of confined fluids approximately collapses onto a single curve that can be described by the Langevin function. In this subfigure, the scaled perpendicular permittivity is defined as $\tilde{\varepsilon}_{\perp} = \frac{\varepsilon_{\perp} - \varepsilon_{sl}}{\varepsilon_b - \varepsilon_{sl}}$, and the scaled channel width is given by $\widetilde{H} = \frac{H - H_{sl}}{\sigma_d(\varepsilon_b - \varepsilon_{sl})}$.

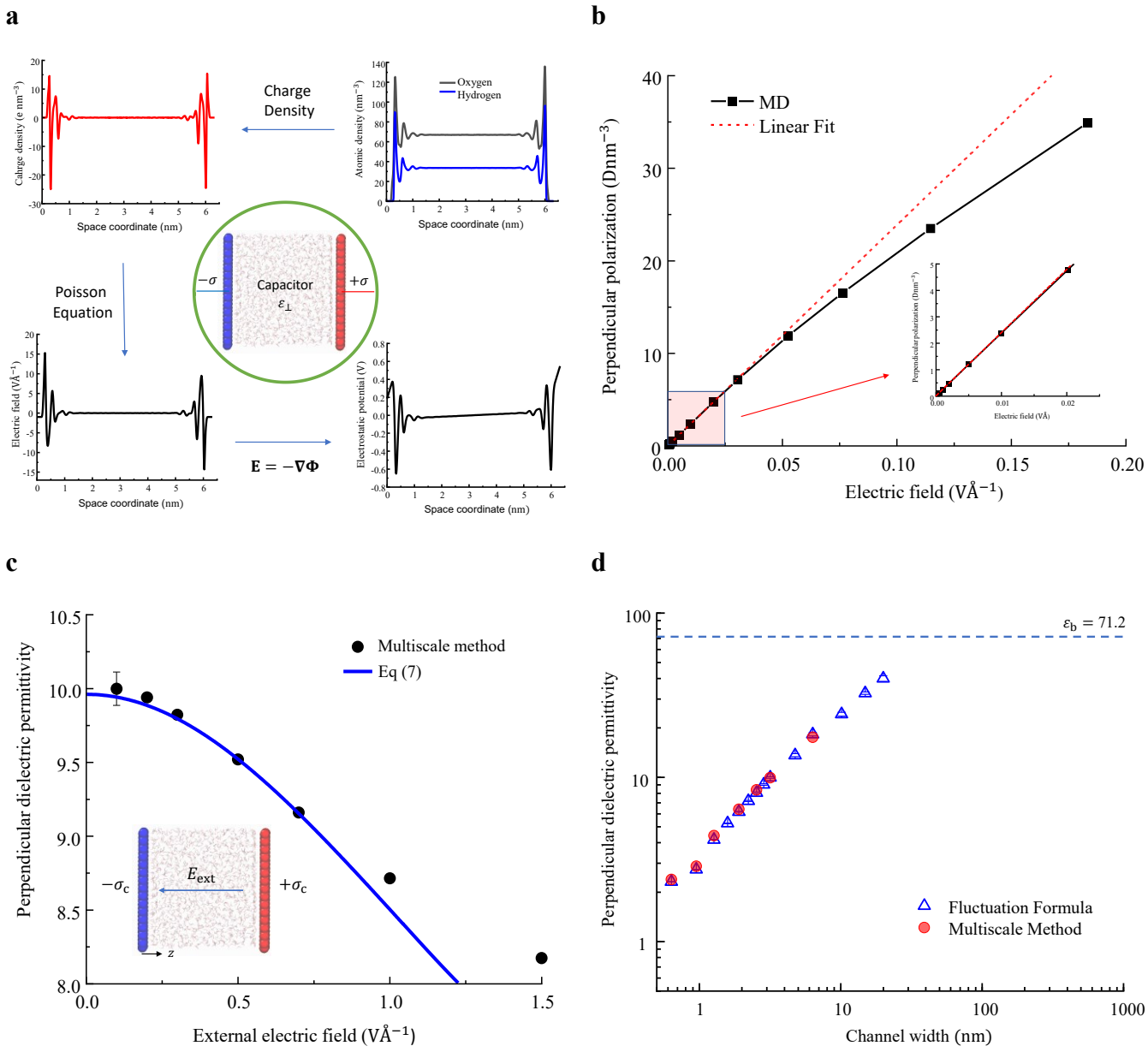

Figure 2. Parallel-plate capacitor multiscale method. **(a)** Schematic procedure for calculating the perpendicular dielectric permittivity of confined fluids using eq (6). The procedure is illustrated for water, where we first calculate the density of oxygen and hydrogen atoms. Multiplying by their atomic charges, we obtain the charge density profile which can be used in the Poisson equation to obtain electric field and thus the electrostatic potential required to calculate the perpendicular dielectric permittivity. **(b)** Total

perpendicular polarization density ($p_\perp = P_\perp/V$, where $P_\perp$ is calculated from eq (10)) of water as a function of the electric field for 3.17 nm wide channel. The inset shows the region, where the variation is almost linear and the dielectric constant is nearly independent of the electric field inside the channel. The onset of the nonlinear behavior occurs at the electric field ~0.02 $V\text{Å}^{-1}$ ($E_{ext} = 0.2\, V\text{Å}^{-1}$). **(c)** Electric-field dependent perpendicular dielectric permittivity of water confined in 3.17 nm wide channel for various external electric field strengths. As shown, the direction of the applied electric field is from right to left. Filled circles are calculated from eq (6) and the line is the fitted curve using eq (7) with the following fitting parameters: $b = 1.78 \pm 0.03\ \text{Å}V^{-1}$, and $\varepsilon_\perp(0) = 9.96 \pm 0.02$ **(d)** Comparison between the water perpendicular dielectric permittivity obtained at the limit of zero electric field from the multiscale parallel-plate capacitor method *versus* the results obtained from the fluctuation formula.

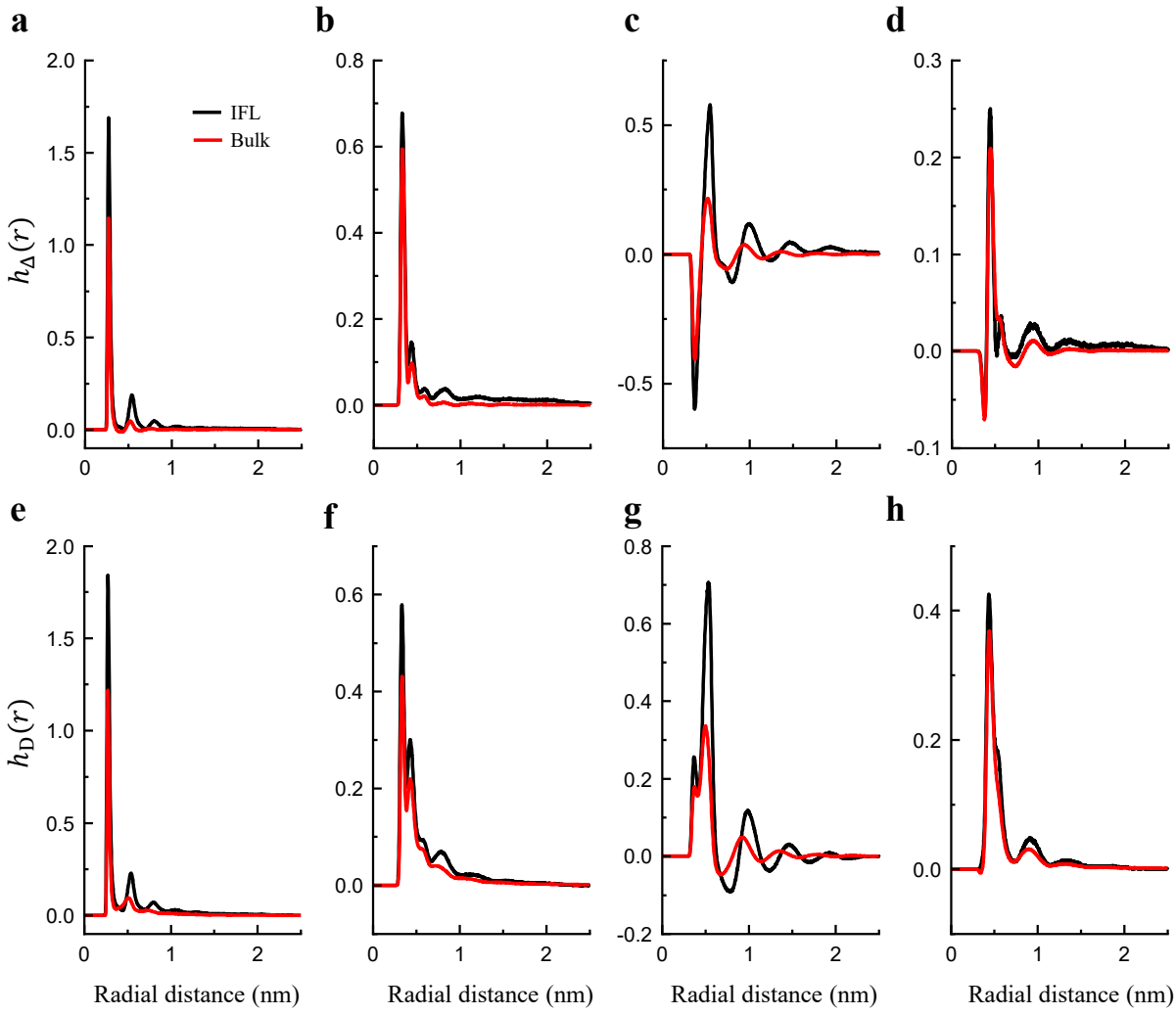

Figure 3. Dipolar orientational correlation functions. Dipolar correlations for water (a,e), methanol (b,f), acetonitrile (c,g), and dichloromethane (d,h). The top row shows the dipole-dipole pair correlation function and the bottom row shows the angular dependence of the dipole-dipole interaction energy in bulk (red color) and in the interfacial layer next to the graphene surface (black color) as a function of the separation distance r. It is important to note that in IFL the distance between the dipoles lies in the xy plane (parallel to the surface). Therefore, the separation distance is the in-plane radial distance, *i.e.,* $\boldsymbol{r}_{||} = (x, y)$.

References

(1) Sugahara, A.; Ando, Y.; Kajiyama, S.; Yazawa, K.; Gotoh, K.; Otani, M.; Okubo, M.; Yamada, A. Negative Dielectric Constant of Water Confined in Nanosheets. *Nat. Commun.* **2019**, *10*, 1–7.

(2) Li, C. P.; Du, M. Role of Solvents in Coordination Supramolecular Systems. *Chem. Commun.* **2011**, *47*, 5958–5972.

(3) Noyes, R. M. Thermodynamics of Ion Hydration as a Measure of Effective Dielectric Properties of Water. *J. Am. Chem. Soc.* **1962**, *84*, 513–522.

(4) Uematsu, Y.; Netz, R. R.; Bonthuis, D. J. Analytical Interfacial Layer Model for the Capacitance and Electrokinetics of Charged Aqueous Interfaces. *Langmuir* **2018**, *34*, 9097–9113.

(5) Faucher, S.; Aluru, N.; Bazant, M. Z.; Blankschtein, D.; Brozena, A. H.; Cumings, J.; Pedro De Souza, J.; Elimelech, M.; Epsztein, R.; Fourkas, J. T.; Rajan, A. G.; Kulik, H. J.; Levy, A.; Majumdar, A.; Martin, C.; McEldrew, M.; Misra, R. P.; Noy, A.; Pham, T. A.; Reed, M. *et al.* Critical Knowledge Gaps in Mass Transport through Single-Digit Nanopores: A Review and Perspective. *J. Phys. Chem. C* **2019**, *123*, 21309–21326.

(6) Ahmad, M.; Gu, W.; Geyer, T.; Helms, V. Adhesive Water Networks Facilitate Binding of Protein Interfaces. *Nat. Commun.* **2011**, *2*.

(7) Bellissent-Funel, M.-C.; Hassanali, A.; Havenith, M.; Henchman, R.; Pohl, P.; Sterpone, F.; van der Spoel, D.; Xu, Y.; Garcia, A. E. Water Determines the Structure and Dynamics of Proteins. *Chem. Rev.* **2016**, *116*, 7673–7697.

(8) Shannon, M.; Bohn, P.; Elimelech, M.; Georgiadis, J. G.; Mariñas, B. J.; Mayes, A. M. Science and Technology for Water Purification in the Coming Decades. *Nature* **2008**, *452*, 301–310.

(9) Heiranian, M.; Farimani, A. B.; Aluru, N. R. Water Desalination with a Single-Layer MoS 2 Nanopore. *Nat. Commun.* **2015**, *6*, 1–6.

(10) Toney, M. F.; Howard, J. N.; Richer, J.; Borges, G. L.; Gordon, J. G.; Melroy, O. R.; Wiesler, D. G.; Yee, D.; Sorensen, L. B. Voltage-Dependent Ordering of Water Molecules at an Electrode-Electrolyte Interface. *Nature* **1994**, *368*, 444–446.

(11) Algara-Siller, G.; Lehtinen, O.; Wang, F. C.; Nair, R. R.; Kaiser, U.; Wu, H. A.; Geim, A. K.; Grigorieva, I. V. Square Ice in Graphene Nanocapillaries. *Nature* **2015**, *519*, 443–445.

(12) Ballenegger, V.; Hansen, J. P. Dielectric Permittivity Profiles of Confined Polar Fluids. *J. Chem. Phys.* **2005**, *122*, 1–10.

(13) Bonthuis, D. J.; Gekle, S.; Netz, R. R. Dielectric Profile of Interfacial Water and Its Effect on Double-Layer Capacitance. *Phys. Rev. Lett.* **2011**, *107*, 166102.

(14) Muñoz-Santiburcio, D.; Marx, D. Nanoconfinement in Slit Pores Enhances Water Self-Dissociation. *Phys. Rev. Lett.* **2017**, *119*, 1–6.

(15) Sirkin, Y. A. P.; Hassanali, A.; Scherlis, D. A. One-Dimensional Confinement Inhibits Water Dissociation in Carbon Nanotubes. *J. Phys. Chem. Lett.* **2018**, *9*, 5029–5033.

(16) Duchamp, M.; Lee, K.; Dwir, B.; Seo, J. W.; Kapon, E.; Forró, L.; Magrez, A. Controlled Positioning of Carbon Nanotubes by Dielectrophoresis: Insights into the Solvent and

Substrate Role. *ACS Nano* **2010**, *4*, 279–284.

(17) Motevaselian, M. H.; Mashayak, S. Y.; Aluru, N. R. Extended Coarse-Grained Dipole Model for Polar Liquids: Application to Bulk and Confined Water. *Phys. Rev. E* **2018**, *98*, 052135.

(18) Jadhao, V.; Solis, F. J.; De La Cruz, M. O. Simulation of Charged Systems in Heterogeneous Dielectric Media *via* a True Energy Functional. *Phys. Rev. Lett.* **2012**, *109*, 1–5.

(19) Bonthuis, D. J.; Gekle, S.; Netz, R. R. Profile of the Static Permittivity Tensor of Water at Interfaces: Consequences for Capacitance, Hydration Interaction and Ion Adsorption. *Langmuir* **2012**, *28*, 7679–7694.

(20) Parez, S.; Předota, M.; Machesky, M. Dielectric Properties of Water at Rutile and Graphite Surfaces: Effect of Molecular Structure. *J. Phys. Chem. C* **2014**, *118*, 4818–4834.

(21) Fumagalli, L.; Esfandiar, A.; Fabregas, R.; Hu, S.; Ares, P.; Janardanan, A.; Yang, Q.; Radha, B.; Taniguchi, T.; Watanabe, K.; Gomila, G.; Novoselov, K. S.; Geim, A. K. Anomalously Low Dielectric Constant of Confined Water. *Science* **2018**, *360*, 1339–1342.

(22) Palmer, L. S.; Cunliffe, A.; Hough, J. M. Dielectric Constant of Water Films. *Nature* **1952**, *170*, 796.

(23) Teschke, O.; Ceotto, G.; de Souza, E. F. Interfacial Water Dielectric-Permittivity-Profile Measurements Using Atomic Force Microscopy. *Phys. Rev. E - Stat. Physics, Plasmas, Fluids, Relat. Interdiscip. Top.* **2001**, *64*, 10.

(24) Loche, P.; Wolde-Kidan, A.; Schlaich, A.; Bonthuis, D. J.; Netz, R. R. Comment on

"Hydrophobic Surface Enhances Electrostatic Interaction in Water." *Phys. Rev. Lett.* **2019**, *123*, 049601.

(25) Kirkwood, J. G. The Dielectric Polarization of Polar Liquids. *J. Chem. Phys.* **1939**, *7*, 911–919.

(26) Fröhlich, H. Theory of Dielectrics. *Phys. Today* **1959**, *12*, 40–42.

(27) Faraudo, J.; Bresme, F. Anomalous Dielectric Behavior of Water in Ionic Newton Black Films. *Phys. Rev. Lett.* **2004**, *92*, 1–4.

(28) Zhang, C.; Gygi, F.; Galli, G. Strongly Anisotropic Dielectric Relaxation of Water at the Nanoscale. *J. Phys. Chem. Lett.* **2013**, *4*, 2477–2481.

(29) De Luca, S.; Kannam, S. K.; Todd, B. D.; Frascoli, F.; Hansen, J. S.; Daivis, P. J. Effects of Confinement on the Dielectric Response of Water Extends up to Mesoscale Dimensions. *Langmuir* **2016**, *32*, 4765–4773.

(30) Ghoufi, A.; Szymczyk, A.; Renou, R.; Ding, M. Calculation of Local Dielectric Permittivity of Confined Liquids from Spatial Dipolar Correlations. *Epl* **2012**, *99*.

(31) Mondal, S.; Bagchi, B. Water in Carbon Nanotubes: Pronounced Anisotropy in Dielectric Dispersion and Its Microscopic Origin. *J. Phys. Chem. Lett.* **2019**, *10*, 6287–6292.

(32) Sato, T.; Sasaki, T.; Ohnuki, J.; Umezawa, K.; Takano, M. Hydrophobic Surface Enhances Electrostatic Interaction in Water. *Phys. Rev. Lett.* **2018**, *121*, 206002.

(33) Schlaich, A.; Knapp, E. W.; Netz, R. R. Water Dielectric Effects in Planar Confinement. *Phys. Rev. Lett.* **2016**, *117*, 1–5.

(34) Neumann, M.; Steinhauser, O.; Stuart Pawley, G. Consistent Calculation of the Static and Frequency-Dependent Dielectric Constant in Computer Simulations. *Mol. Phys.* **1984**, *52*, 97–113.

(35) Sharma, M.; Resta, R.; Car, R. Dipolar Correlations and the Dielectric Permittivity of Water. *Phys. Rev. Lett.* **2007**, *98*, 247401.

(36) Chmiola, J.; Yushin, G.; Gogotsi, Y.; Portet, C.; Simon, P.; Taberna, P. L. Anomalous Increase in Carbon at Pore Sizes Less than 1 Nanometer. *Science* **2006**, *313*, 1760–1763.

(37) Merlet, C.; Péan, C.; Rotenberg, B.; Madden, P. A.; Daffos, B.; Taberna, P. L.; Simon, P.; Salanne, M. Highly Confined Ions Store Charge More Efficiently in Supercapacitors. *Nat. Commun.* **2013**, *4*, 2–7.

(38) Aragones, J. L.; MacDowell, L. G.; Vega, C. Dielectric Constant of Ices and Water: A Lesson about Water Interactions. *J. Phys. Chem. A* **2011**, *115*, 5745–5758.

(39) Booth, F. The Dielectric Constant of Water and the Saturation Effect. *J. Chem. Phys.* **1951**, *19*, 391–394.

(40) Booth, F. Errata: The Dielectric Constant of Water and the Saturation Effect. *J. Chem. Phys.* **1951**, *19*, 1327–1328.

(41) Daniels, I. N.; Wang, Z.; Laird, B. B. Dielectric Properties of Organic Solvents in an Electric Field. *J. Phys. Chem. C* **2017**, *121*, 1025–1031.

(42) Gavish, N.; Promislow, K. Dependence of the Dielectric Constant of Electrolyte Solutions on Ionic Concentration: A Microfield Approach. *Phys. Rev. E* **2016**, *94*, 1–7.

(43) Heid, E.; Docampo-Álvarez, B.; Varela, L. M.; Prosenz, K.; Steinhauser, O.; Schröder, C. Langevin Behavior of the Dielectric Decrement in Ionic Liquid Water Mixtures. *Phys. Chem. Chem. Phys.* **2018**, *20*, 15106–15117.

(44) Mashayak, S. Y.; Aluru, N. R. Langevin-Poisson-EQT: A Dipolar Solvent Based Quasi-Continuum Approach for Electric Double Layers. *J. Chem. Phys.* **2017**, *146*, 044108.

(45) Ben-Amotz, D.; Herschbach, D. R. Estimation of Effective Diameters for Molecular Fluids. *J. Phys. Chem.* **1990**, *94*, 1038–1047.

(46) De Luca, S.; Kannam, S. K.; Todd, B. D.; Frascoli, F.; Hansen, J. S.; Daivis, P. J. Effects of Confinement on the Dielectric Response of Water Extends up to Mesoscale Dimensions. *Langmuir* **2016**, *32*, 4765–4773.

(47) Stengel, M.; Spaldin, N. A. Origin of the Dielectric Dead Layer in Nanoscale Capacitors. *Nature* **2006**, *443*, 679–682.

(48) Chang, L. W.; Alexe, M.; Scott, J. F.; Gregg, J. M. Settling the "Dead Layer" Debate in Nanoscale Capacitors. *Adv. Mater.* **2009**, *21*, 4911–4914.

(49) Duignan, T. T.; Zhao, X. S. Impurities Limit the Capacitance of Carbon-Based Supercapacitors. *J. Phys. Chem. C* **2019**, *123*, 4085–4093.

(50) Varghese, S.; Kannam, S. K.; Hansen, J. S.; Sathian, S. P. Effect of Hydrogen Bonds on the Dielectric Properties of Interfacial Water. *Langmuir* **2019**, *35*, 8159–8166.

(51) Terrones, J.; Kiley, P. J.; Elliott, J. A. Enhanced Ordering Reduces Electric Susceptibility of Liquids Confined to Graphene Slit Pores. *Sci. Rep.* **2016**, *6*, 1–11.

(52) Abraham, M. J.; Murtola, T.; Schulz, R.; Páll, S.; Smith, J. C.; Hess, B.; Lindah, E. Gromacs: High Performance Molecular Simulations through Multi-Level Parallelism from Laptops to Supercomputers. *SoftwareX* **2015**, *1–2*, 19–25.

(53) Nosé, S. A Unified Formulation of the Constant Temperature Molecular Dynamics Methods. *J. Chem. Phys.* **1984**, *81*, 511.

(54) Chialvo, A. A.; Cummings, P. T. Molecular-Based Modeling of Water and Aqueous Solutions at Supercritical Conditions. *Adv. Chem. Phys.* **1999**, *109*, 115–206.

(55) Darden, T.; York, D.; Pedersen, L. Particle Mesh Ewald: An N·log(N) Method for Ewald Sums in Large Systems. *J. Chem. Phys.* **1993**, *98*, 10089–10092.

(56) Yeh, I. C.; Berkowitz, M. L. Ewald Summation for Systems with Slab Geometry. *J. Chem. Phys.* **1999**, *111*, 3155–3162.

(57) Ryckaert, J. P.; Ciccotti, G.; Berendsen, H. J. C. Numerical Integration of the Cartesian Equations of Motion of a System with Constraints: Molecular Dynamics of *n*-Alkanes. *J. Comput. Phys.* **1977**, *23*, 327–341.

(58) Nikitin, A. M.; Lyubartsev, A. P. New Six-Site Acetonitrile Model for Simulations of Liquid Acetonitrile and Its Aqueous Mixtures. *J. Comput. Chem.* **2007**, *28*, 2020–2026.

(59) Caleman, C.; Van Maaren, P. J.; Hong, M.; Hub, J. S.; Costa, L. T.; Van Der Spoel, D. Force Field Benchmark of Organic Liquids: Density, Enthalpy of Vaporization, Heat Capacities, Surface Tension, Isothermal Compressibility, Volumetric Expansion Coefficient, and Dielectric Constant. *J. Chem. Theory Comput.* **2012**, *8*, 61–74.

(60) Liu, Z.; Timmermann, J.; Reuter, K.; Scheurer, C. Benchmarks and Dielectric Constants for Reparametrized OPLS and Polarizable Force Field Models of Chlorinated Hydrocarbons. *J. Phys. Chem. B* **2018**, *122*, 770–779.

(61) Stern, H. A.; Feller, S. E. Calculation of the Dielectric Permittivity Profile for a Nonuniform System: Application to a Lipid Bilayer Simulation. *J. Chem. Phys.* **2003**, *118*, 3401–3412.

For Table of Contents Only: